# Effect of off-stoichiometric composition on half-metallic character of $Co_2Fe(Ga,Ge)$ investigated using saturation magnetization and giant magnetoresistance effect

Yuki Chikaso[1], Masaki Inoue[1], Tessei Tanimoto[1], Keita Kikuchi[1], Michihiko Yamanouchi[1], Tetsuya Uemura[1], Kazuumi Inubushi[2], Katsuyuki Nakada[2], Hikari Shinya[3,4,5] and Masafumi Shirai[3,4]

1 Graduate School of Information Science and Technology, Hokkaido University, Sapporo 060-0814, Japan

2 Advanced Products Development Center, Technology & Intellectual Property HQ, TDK Corporation, Ichikawa 272-8558, Japan

3 Research Institute of Electrical Communication, Tohoku University, Sendai 980-8577, Japan

4 Center for Spintronics Research Network, Tohoku University, Sendai 980-8577, Japan

5 Center for Spintronics Research Network, Osaka University, Toyonaka 560-8531, Japan

E-mail: uemura@ist.hokudai.ac.jp

## Abstract

We investigated the Ge-composition ($\gamma$) dependence of the saturation magnetization of CFGG thin films and the magnetoresistance (MR) ratio of CFGG-based current-perpendicular-to-plane giant magnetoresistance (CPP-GMR) devices together with first-principles calculations of the electronic states of CFGG. Theoretical calculations showed that spin polarization is highest at the stoichiometric composition $\gamma$ = 0.56 in

$Co_2Fe_{1.03}Ga_{0.41}Ge_\gamma$ and that it decreases in off-stoichiometric CFGG, mainly due to the formation of $Co_{Fe}$ antisites for Ge-deficient compositions and $Fe_{Co}$ antisites for Ge-rich compositions, where $Co_{Fe}$ ($Fe_{Co}$) indicates that Co (Fe) atoms replace the Fe (Co) sites. The saturation magnetic moment ($\mu_s$) per formula unit decreased monotonically as $\gamma$ increased from 0.24 to 1.54 in $Co_2Fe_{1.03}Ga_{0.41}Ge_\gamma$. The $\mu_s$ was closest to the Slater-Pauling value predicted for half-metallic CFGG at the stoichiometric composition $\gamma$ = 0.56, indicating that stoichiometric CFGG has a half-metallic nature. This is consistent with the result for the theoretical spin polarization. In contrast, the MR ratio of CFGG-based CPP-GMR devices increased monotonically as $\gamma$ increased from 0.24 to 1.10 and reached an MR ratio of 87.9% at the Ge-rich composition $\gamma$ = 1.10. Then, the MR ratio decreased rapidly as $\gamma$ increased from 1.10 to 1.48. Possible origins for the slight difference between the Ge composition at which the highest MR ratio was obtained ($\gamma$ = 1.10) and that at which the highest spin polarization was obtained ($\gamma$ = 0.56) are improved atomic arrangements in a Ge-rich CFGG film and the reduction of effective Ge composition due to Ge diffusion in the GMR stacks.

Keywords: Heusler alloy thin films, half-metallic character, giant magnetoresistance, $Co_2Fe(Ga, Ge)$

## I. INTRODUCTION

Magneto-resistive (MR) devices with low device resistance and a high output signal are indispensable for use as read sensors in next-generation hard disk drives [1]. A current-perpendicular-to-plane (CPP) giant magnetoresistance (GMR) device using Co-based Heusler alloy ($Co_2YZ$, where Y is usually a transition metal and Z is a main group element) is a promising candidate for such devices [2–17]. This is because many Co-based Heusler alloys, such as $Co_2MnSi$ (CMS) and $Co_2MnGe$ (CMG), have theoretically 100% spin polarization at Fermi level ($E_F$) due to their half-metallic nature, which is characterized by an energy gap for one spin direction at $E_F$ [18–22]. Furthermore, such alloys have relatively high Curie temperatures, well above room temperature (RT) [23], so a high MR ratio is expected in GMR devices, even at or above RT.

To take full advantage of the half-metallic character of $Co_2YZ$, it is of great importance to suppress the structural defects harmful to the half-metallicity. In particular, $Co_{Y(Z)}$ antisites, where Co atoms have replaced Y(Z) sites, should be suppressed because the hybridized orbitals between Co atoms located at the second nearest neighbors in the $L2_1$-ordered structure are the origin of the half-metal gap [21]. First-principles calculations showed that $Co_{Mn}$ antisites in CMS and CMG can cause minority-spin in-gap states at $E_F$ and thus are detrimental to the half-metallicity of CMS and CMG [24]. Similarly, $Co_{Cr}$ antisites in $Co_2CrAl$ have been shown to lead to a substantial reduction in spin polarization at $E_F$ [25].

Note that off-stoichiometry and/or structural defects are inevitable in ternary or quaternary Co-based Heusler alloy thin films prepared by magnetron sputtering or molecular beam epitaxy. Increasing the Y or Z composition in $Co_2YZ$ is a highly effective way to suppress $Co_{Y(Z)}$ antisites. Recently an enhancement of tunneling

magnetoresistance (TMR) ratios was demonstrated in Mn-rich or (Mn + Fe)-rich off-stoichiometric CMS-based magnetic tunnel junctions (MTJs), CMG-based MTJs, and $Co_2$(Mn,Fe)Si (CMFS)-based MTJs [26–29]. In particular, high TMR ratios of 1995% at 4.2 K and 354% at 290 K were achieved for Mn-rich CMS-based MTJs [27], and ones of 2610% at 4.2 K and 429% at 290 K were achieved for (Mn + Fe)-rich CMFS-based MTJs [29]. Moreover, the effects of $Co_{Mn}$ antisites on half-metallicity have been studied through investigations of saturation magnetization per formula unit [30,31], surface spin polarization [32], electronic and/or magnetic states [33–38], and Gilbert damping constants [39]. These studies showed that $Co_{Mn}$ antisites can be suppressed by increasing the Mn or Mn + Fe compositions of these materials.

In contrast, enhancement of the MR ratio by increasing the Mn composition in CMS-based CPP-GMR devices has been limited; the maximum MR ratio was approximately 20% at 290 K in Mn-rich CMS-based CPP-GMR devices [13] due to a reduction in the spin diffusion length of the Ag spacer and the presence of a biquadratic interlayer exchange coupling between the upper and lower CMS electrodes. Both effects originated from the diffusion of Mn atoms into the spacer [14]. In contrast, a relatively high MR ratio of 82% at 290 K has been reported for Mn-free $Co_2$Fe(Ga, Ge) (CFGG)-based CPP-GMR devices [11]. However, the effect of controlling the composition of CFGG films on MR characteristics has not been clarified yet.

In this study, we investigated the effect of off-stoichiometry on the half-metallic character of CFGG by using the Ge-composition dependence of the saturation magnetic moment ($\mu_s$) per formula unit of CFGG thin films and the MR ratio of CFGG-based CPP-GMR devices. Moreover, we performed the first-principles calculations of the electronic states of CFGG with off-stoichiometric compositions.

This paper is organized as follows. Section II presents the experimental and computational methods. To calculate the electronic structures of off-stoichiometric CFGG, a site-specific formula unit (SSFU) composition model was developed. Section III presents the results and discussion. Section III A describes the first-principles calculations of the electronic states of CFGG with various Ge compositions. Section III B describes the Ge-composition dependence of both the experimental and theoretical $\mu_s$ of CFGG thin films. Section III C describes the Ge-composition dependence of the atomic order of the CFGG lower electrode and the MR characteristics of CFGG-based CPP-GMR devices. Section III D discusses the origin of the Ge-composition dependence of the MR ratio in comparison with the theoretical spin polarization. Section IV summarizes our results and concludes the paper.

## II. EXPERIMENTAL AND COMPUTATIONAL METHODS

### A. Experimental methods

We prepared three series of CFGG-based CPP-GMR devices with an Ag spacer. The layer structure of the series-A GMR devices was (from the substrate side) MgO buffer (10 nm)/$Co_{50}Fe_{50}$ seed (10)/Ag buffer (100)/CFGG lower electrode (10)/Ag spacer (5)/CFGG upper electrode (8)/Ru cap layer (5), grown on a (001)-oriented MgO single crystalline substrate. The numbers in parentheses are the nominal thicknesses in nanometers. For the series-B and -C ones, a 0.21-nm-thick ultrathin NiAl layer was inserted at the interfaces of the spacer with the upper and lower CFGG electrodes, with the aim of enhancing the MR ratio [11]. The Ge composition $\gamma$ was systematically varied in each series. Since it is desirable to include a stoichiometric one among them, the composition ratio of Co and Fe was fixed to be approximately 2:1. The $\gamma$ of $Co_2Fe_{1.03}Ga_{0.41}Ge_\gamma$ was varied from 0.24 to

1.06 for series-A and from 0.56 to 1.06 for series-B. The $\gamma$ of $Co_2Fe_{1.09}Ga_{0.46}Ge_\gamma$ was varied from 1.10 to 1.48 for series-C.

The CFGG films were deposited at RT using radio-frequency magnetron co-sputtering from a nearly stoichiometric CFGG target and a Ge target. Immediately after deposition of the upper CFGG electrode, the layer structures were *in-situ* annealed at 550˚C for 15 min to improve atomic ordering. The layer structures and annealing condition were optimized in terms of MR ratio (see Fig. S1 in Supplementary Data). Each layer was successively deposited in an ultrahigh vacuum chamber with a base pressure of about 7 $\times 10^{-8}$ Pa. Epitaxial growth of each layer was confirmed by *in-situ* reflection high-energy electron diffraction observation.

The film composition of the prepared CFGG film was determined by inductively coupled plasma (ICP) analysis. The lower and upper CFGG electrodes in the GMR layer structures were characterized by cross-sectional high-angle annular dark-field scanning transmission electron microscope (HAADF-STEM) lattice image observation and convergent-beam electron diffraction (CBED) observations. We also prepared a series of 30-nm-thick $Co_2Fe_{1.03}Ga_{0.41}Ge_\gamma$ films with various values of $\gamma$ ranging from 0.24 to 1.54 to evaluate the saturation magnetic moment.

We fabricated CPP-GMR devices with nominal junction sizes ranging from 55 × 90 nm to 400 × 640 nm by using electron beam lithography and Ar ion milling. The MR characteristics were measured using a dc four-probe method by sweeping the magnetic field at 290 K. The typical voltage across the junction was 1 mV or less to suppress Joule heating. The MR ratios were defined as $(R_{AP} - R_P)/R_P$, where $R_P$ and $R_{AP}$ are the junction resistances for the parallel and antiparallel magnetization configurations between the upper and lower CFGG electrodes.

### B. Computational method

To examine the defect formation energies, we performed density functional theory calculations [40,41] using Vienna *ab initio* simulation package (VASP) code [42–44] based on the projector augmented wave method [45]. We used a supercell containing 32 atomic positions, occupied by 16 Co, 8 Fe, 4 Ga, and 4 Ge atoms. In these calculations, we used a 6 × 6 × 6 Monkhorst-Pack [46] *k*-point mesh and set the plane-wave cutoff energy to 450 eV. The Perdew-Becke-Erzenhof (PBE) approach [47] to the generalized gradient approximation (GGA) for the exchange-correlation functional was used. We determined the favorable atomic arrangement in a formula unit for off-stoichiometric CFGG as described in the next section.

For the electronic structures and magnetic properties of off-stoichiometric CFGG systems, we used the Korringa–Kohn–Rostoker (KKR) Green function method [48,49] with the coherent potential approximation (CPA) [50,51], implemented in the AkaiKKR program package [52]. We used the variational pseudo self-interaction correction (VPSIC) method [53] with local density approximation (LDA) to describe the localized 3d orbitals. We chose 256 *k*-sampling points in the first irreducible Brillouin zone. The relativistic effects were included by scalar relativistic approximation [54].

### C. Site-specific formula unit composition model

To clarify the half-metallicity of the off-stoichiometric Co-based Heusler alloys, it is essential to understand the disorder of their crystal structure. To do this, the SSFU composition model was previously developed for off-stoichiometric CMS and CMFS [27,30,31]. In accordance with the theoretically predicted formation energies of various defects induced in CMS [55], this model is based on the assumption that antisite defects,

not vacancies, form to accommodate off-stoichiometric CMS and CMFS.

In this study, we calculated the formation energies of various defects for CFGG and found that those of antisite defects of $Co_{Fe}$, $Fe_{Co}$, $Fe_{(Ga,Ge)}$, and $(Ga,Ge)_{Fe}$, where $X_Y$ indicates that a Y site is replaced by an X atom, are lower than those of other defects, such as vacancies. We thus assumed the presence of only these antisite defects in the SSFU model for CFGG. In this model, each site in the $L2_1$ structure is occupied either by the nominal atom (Co, Fe, or Ga/Ge for CFGG) for that site or by an antisite defect atom. Therefore, the total number of atoms included in the formula unit is always four, even though the film is off-stoichiometric in terms of the Co:Fe:Ga/Ge atomic ratio.

The SSFU compositions are categorized into four types, summarized in Table I, depending on the values of $\alpha$, $\beta$, and $\gamma$ in $Co_2Fe_\alpha Ga_\beta Ge_\gamma$. For example, if $2 - (\alpha + \beta + \gamma) \geq 0$ and $3(\beta + \gamma) - (2 + \alpha) \geq 0$, an Fe site is replaced by Co and $Ga_{1-\xi}Ge_\xi$ by an amount of $x$ and $y$, respectively, where $x = |2\{2 - (\alpha + \beta + \gamma)\}/(2 + \alpha + \beta + \gamma)|$, $y = |\{3(\beta + \gamma) - (2 + \alpha)\}/(2 + \alpha + \beta + \gamma)|$, and $\xi = \gamma/(\beta + \gamma)$, resulting in the SSFU composition of $[Co_2][Co_xFe_{1-x-y}(Ga_{1-\xi}Ge_\xi)_y][Ga_{1-\xi}Ge_\xi]$ (Type-I). Note that $Co_{Fe}$ antisites exist in type-I and -II, whereas $Fe_{Co}$ antisites exist in type-III and -IV. The details of SSFU model are described at §2 in Supplementary Data.

We calculated electronic states for a series of $Co_2Fe_{1.03}Ga_{0.41}Ge_\gamma$ with various values of $\gamma$ ranging from 0.24 to 1.54. Table II summarizes their SSFU compositions together with the SSFU type.

Table I. General expressions for SSFU compositions of off-stoichiometric $Co_2Fe_\alpha Ga_\beta Ge_\gamma$, where $x = |2\{2 - (\alpha + \beta + \gamma)\}/(2 + \alpha + \beta + \gamma)|$, $y = |\{3(\beta + \gamma) - (2 + \alpha)\}/(2 + \alpha + \beta + \gamma)|$, and $\xi = \gamma/(\beta + \gamma)$.

| SSFU type | Conditions | SSFU composition |
|---|---|---|
| I | $2 - (\alpha + \beta + \gamma) \geq 0$<br>$3(\beta + \gamma) - (2 + \alpha) \geq 0$ | $[Co_2]\,[Co_xFe_{1-x-y}(Ga_{1-\xi}Ge_\xi)_y]\,[Ga_{1-\xi}Ge_\xi]$ |
| II | $2 - (\alpha + \beta + \gamma) \geq 0$<br>$3(\beta + \gamma) - (2 + \alpha) \leq 0$ | $[Co_2]\,[Co_xFe_{1-x}]\,[Fe_y(Ga_{1-\xi}Ge_\xi)_{1-y}]$ |
| III | $2 - (\alpha + \beta + \gamma) \leq 0$<br>$3(\beta + \gamma) - (2 + \alpha) \geq 0$ | $[Co_{2-x}Fe_x]\,[Fe]\,[Fe_y\,(Ga_{1-\xi}Ge_\xi)_{1-y}]$ |
| IV | $2 - (\alpha + \beta + \gamma) \leq 0$<br>$3(\beta + \gamma) - (2 + \alpha) \leq 0$ | $[Co_{2-x}Fe_x]\,[Fe_{1-y}(Ga_{1-\xi}Ge_\xi)_y]\,[Ga_{1-\xi}Ge_\xi]$ |

Table II. SSFU compositions of off-stoichiometric $Co_2Fe_{1.03}Ga_{0.41}Ge_\gamma$.

| $\gamma$ | SSFU type | SSFU composition |
|---|---|---|
| 0.24 | II | $[Co_2][Fe_{0.826}Co_{0.174}][Ga_{0.446}Ge_{0.261}Fe_{0.293}]$ |
| 0.56 | II | $[Co_2][Fe][Ga_{0.410}Ge_{0.560}Fe_{0.03}]$ |
| 0.96 | IV | $[Co_{1.818}Fe_{0.182}][Fe_{0.755}Ga_{0.073}Ge_{0.172}][Ga_{0.299}Ge_{0.701}]$ |
| 1.25 | IV | $[Co_{1.706}Fe_{0.294}][Fe_{0.584}Ga_{0.103}Ge_{0.313}][Ga_{0.247}Ge_{0.753}]$ |
| 1.54 | IV | $[Co_{1.606}Fe_{0.394}][Fe_{0.434}Ga_{0.119}Ge_{0.447}][Ga_{0.210}Ge_{0.790}]$ |

## III. RESULTS AND DISCUSSION

### A. Effect of off-stoichiometric composition on electronic states of CFGG

To clarify the effect of an off-stoichiometric composition on the electronic states of CFGG, we theoretically investigated the Ge-composition dependence of the spin polarization of CFGG by using KKR-CPA calculations based on the SSFU composition model. Figure 1 shows (a) the theoretical spin polarization, $P_{th}(spd)$ and $P_{th}(sp)$, and (b) the total density of state (DOS) calculated for $Co_2Fe_{1.03}Ga_{0.41}Ge_\gamma$ for various $\gamma$ values, where $P_{th}(spd)$ was determined by considering all the contributions from *s*-, *p*-, and *d*-like electrons for the majority- and minority-spin DOS at $E_F$, and $P_{th}(sp)$ was calculated from DOS for the *s*- and *p*-like electrons. A clear energy gap exists at $E_F$ in the minority-spin band for a stoichiometric Ge-composition of $\gamma$ = 0.56 [Fig. 1(b)], resulting in both $P_{th}(spd)$ and $P_{th}(sp)$ having their highest values. However, relatively large minority-spin states appear around $E_F$ for both $\gamma$ = 0.24 (Ge-deficient composition) and $\gamma$ = 0.96 (Ge-rich composition), resulting in the decrease of $P_{th}(spd)$ and $P_{th}(sp)$.

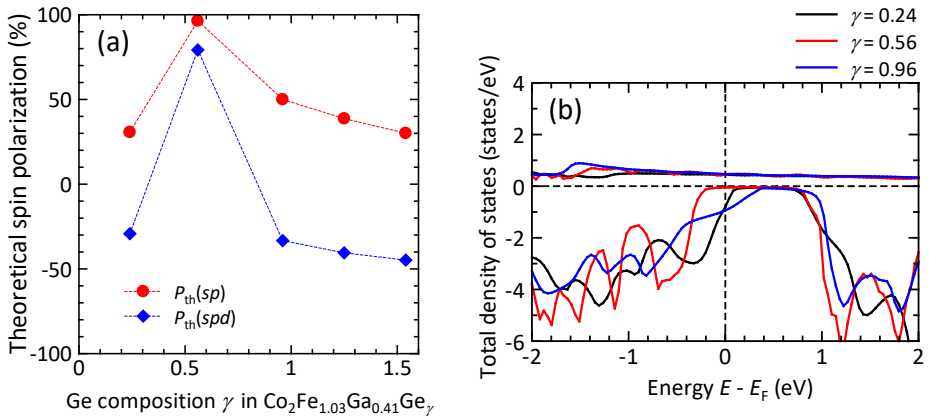


FIG. 1. (a) Theoretical spin polarization at $E_F$ as a function of Ge-composition $\gamma$ in $Co_2Fe_{1.03}Ga_{0.41}Ge_\gamma$. (b) Total density of states of $Co_2Fe_{1.03}Ga_{0.41}Ge_\gamma$ with $\gamma$ = 0.24, 0.56, and 0.96.

Figures 2(a)–(d) show the local DOS for Co at its ordinary site ($Co_{Co}$), Fe at its ordinary site ($Fe_{Fe}$), Co at an Fe antisite ($Co_{Fe}$), and Fe at a Co antisite ($Fe_{Co}$), which can help us understand the decrease in spin polarization for off-stoichiometric Ge compositions. For the CFGG with Ge-deficient composition of $\gamma$ = 0.24 (SSFU composition of $Co_2[Fe_{0.826}Co_{0.174}][Ga_{0.446}Ge_{0.261}Fe_{0.293}]$), the existence of $Co_{Fe}$ antisites decreases the spin polarization due to relatively large minority states appearing around $E_F$ in $Co_{Fe}$ antisites [see Fig. 2(c)]. Moreover, the existence of $Co_{Fe}$ induces a change in the electronic structure of the $Co_{Co}$; that is, it increases the local density of states (LDOS) around $E_F$ in the minority-spin band of the $Co_{Co}$ [see black curve in Fig. 2(a)]. Thus, the decrease in spin polarization for the Ge-deficient CFGG is mainly ascribed to the increase in the LDOS in the minority-spin band of both $Co_{Fe}$ and $Co_{Co}$. This situation is similar to that for Mn-deficient CMS or CMFS, where the spin polarization is dominantly affected by the LDOS of $Co_{Mn}$ and $Co_{Co}$ [30]. More generally, the CFGG for $\gamma \leq 0.56$ is categorized as type II in the SSFU model: $Co_2[Fe_{1-x}Co_x][Z_{1-y}Fe_y]$. The fraction of $Co_{Fe}$ antisites $x$ decreases with increasing $\gamma$, because more Ge atoms occupy Fe sites with increasing $\gamma$, making $Co_{Fe}$ antisites less likely to occur. Thus, the spin polarization increases with increasing $\gamma$ from 0.24 to 0.56.

For CFGG with a Ge-rich composition of $\gamma$ = 0.96 (SSFU composition of $[Co_{1.818}Fe_{0.182}][Fe_{0.755}Ga_{0.073}Ge_{0.172}][Ga_{0.299}Ge_{0.701}]$), there are $Fe_{Co}$ antisites. More generally, the CFGG for $\gamma > 0.56$ is categorized as type IV in the SSFU model, $[Co_{2-x}Fe_x][Fe_{1-y}Z_y][Z]$, and the fraction of $Fe_{Co}$ antisites $y$ increases with increasing Ge composition, because more Ge atoms occupy Fe sites with increasing $\gamma$, making $Fe_{Co}$ antisites likely to occur. The $Fe_{Co}$ antisites with relatively large minority states around $E_F$ [see Fig. 2(d)] reduce the spin polarization. Moreover, the $Fe_{Co}$ antisites also induce an

increase in the LDOS around $E_F$ in the minority-spin band of the $Co_{Co}$ [see blue curve in Fig. 2(a)]. Thus, the decrease in spin polarization for the Ge-rich CFGG is mainly ascribed to the increase in the LDOS in the minority-spin band of both $Fe_{Co}$ and $Co_{Co}$. This contrasts with the case for Mn-rich CMS or CMFS, where $Mn_{Co}$ antisites have little effect on the LDOS in the minority-spin band, and the half-metallicity is kept for a relatively wide range of Mn-rich compositions [24,30,31].

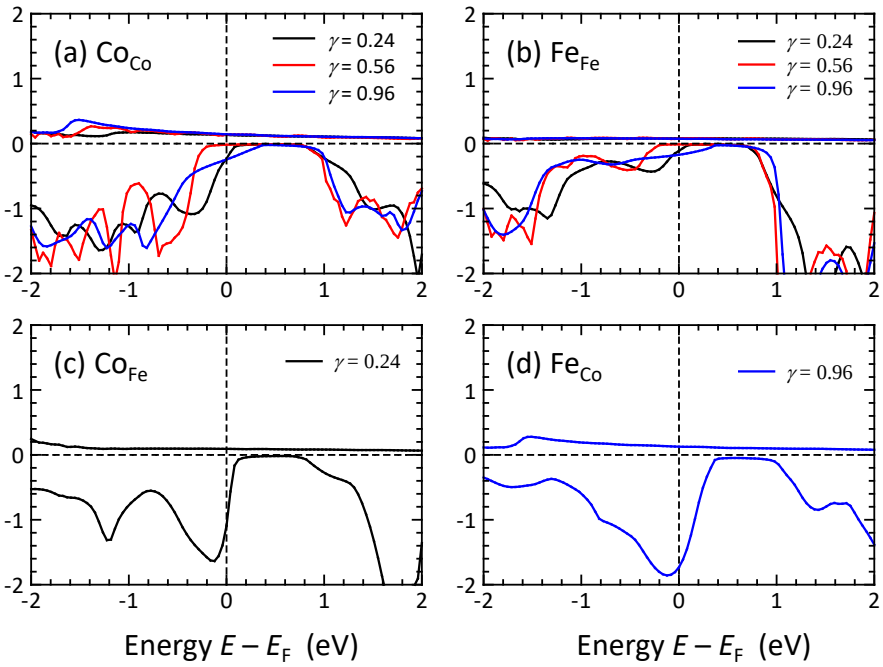


FIG. 2. Local density of states per atom for (a) ordinary-site Co ($Co_{Co}$), (b) ordinary-site Fe ($Fe_{Fe}$), (c) $Co_{Fe}$ antisites, and (d) $Fe_{Co}$ antisites, for CFGG with $\gamma$ = 0.24, 0.56, and 0.96. Note that $Co_{Co}$ and $Fe_{Fe}$ exist at $\gamma$ = 0.24, 0.56, and 0.96, whereas $Co_{Fe}$ antisites exist only at $\gamma$ = 0.24, and $Fe_{Co}$ antisites exist only at $\gamma$ = 0.96 (see Table II).

**B. Effect of off-stoichiometric composition on saturation magnetic moment of CFGG thin films**

We now describe the Ge-composition dependence of $\mu_s$. Figure 3(a) shows typical

magnetic hysteresis curves measured at 4.2 K for $Co_2Fe_{1.03}Ga_{0.41}Ge_\gamma$ thin films with $\gamma$ ranging from 0.24 to 1.54. The saturation magnetization decreased as $\gamma$ increased. Figure 3(b) shows Ge-composition dependence of experimental values of $\mu_s$ per formula unit at 4.2 K for CFGG thin films (blue squares) and the theoretical total spin magnetic moment (red circles). The Slater-Pauling value for half-metallic $Co_2YZ$ alloys, $(Z_t - 24)\mu_B$ [21] was also plotted (solid line), where $Z_t$ is the total number of valence electrons per formula unit provided by the SSFU composition of CFGG and $\mu_B$ is the Bohr magneton. Evaluation of the experimental $\mu_s$ values is described in detail elsewhere [30,31]. The experimental values were well reproduced by the first-principles calculations, indicating the validity of the computational method based on the SSFU composition model. Both the experimental and theoretical values of $\mu_s$ are closest to $(Z_t - 24)\mu_B$ at the stoichiometric composition $\gamma = 0.56$, indicating that the stoichiometric CFGG is close to half-metallic. On the other hand, the values of $\mu_s$ for the off-stoichiometric compositions deviate from $(Z_t - 24)\mu_B$, indicating that the half-metallicity is broken. These results are consistent with the theoretical spin polarization described in Section III A. The deviation of $\mu_s$ values from $(Z_t - 24)\mu_B$ for the off-stoichiometric CFGG thin films is ascribed to the presence of $Co_{Fe}$ or $Fe_{Co}$.

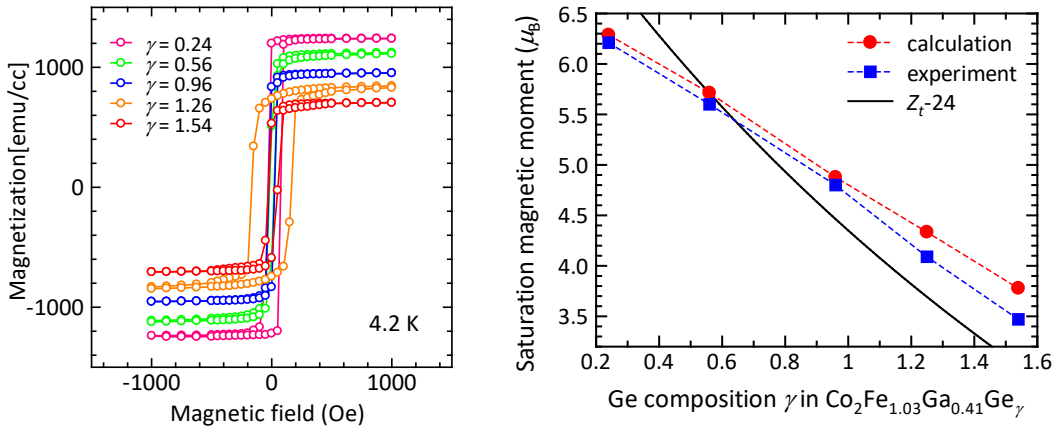


FIG. 3. (a) Typical magnetic hysteresis curves at 4.2 K for $Co_2Fe_{1.03}Ga_{0.41}Ge_\gamma$ ($\gamma$ = 0.24, 0.56, 0.96, 1.26, 1.54) thin films. (b) Ge-composition dependence of experimental saturation magnetic moment per formula unit for CFGG films measured at 4.2 K (blue squares), theoretical total spin magnetic moment (red circles), and Slater-Pauling value, $(Z_t - 24)\mu_B$, predicted for half-metallic CFGG (black solid line).

### C. Effect of off-stoichiometric composition on structural and MR characteristics of CFGG-based GMR devices

First, we describe the effect of off-stoichiometric compositions on the structural properties of $Co_2Fe_{1.03}Ga_{0.41}Ge_\gamma$ films. Figure 4 shows HAADF-STEM lattice images of series-B GMR layer structures with (a) Ge-stoichiometric $Co_2Fe_{1.03}Ga_{0.41}Ge_\gamma$ film with $\gamma$ = 0.56 (SSFU composition of $Co_2Fe_1[Fe_{0.03}Ga_{0.41}Ge_{0.56}]$) and (b) Ge-rich $Co_2Fe_{1.03}Ga_{0.41}Ge_\gamma$ film with $\gamma$ = 1.06 (SSFU composition of $[Co_{1.778}Fe_{0.222}][Fe_{0.693}Ga_{0.086}Ge_{0.221}][Ga_{0.279}Ge_{0.721}]$). Epitaxial growth of CFGG/NiAl/Ag/NiAl/CFGG with clear and abrupt interfaces were confirmed for both films. Moreover, no significant segregation of other phases or materials was observed. This is also supported by x-ray diffraction analysis (see Fig. S2 in Supplementary Data).

To further characterize the effect of the Ge composition on the degree of disorder, CBED patterns for the lower CFGG electrodes are shown in the inset of Figs. 4(a) and (b). For the stoichiometric CFGG film with $\gamma$ = 0.56, 002 diffraction patterns were observed, but no 111 patterns were observed, indicating that the lower CFGG film is B2-orderd (see Table S1 in Supplementary Data). On the other hand, for the Ge-rich CFGG film with $\gamma$ = 1.06, both 002 and 111 diffraction patterns were observed, indicating that the Ge-rich CFGG film is $L2_1$-orderd. Thus, the increase in the Ge composition of off-stoichiometric CFGG effectively improves the atomic order of CFGG films.

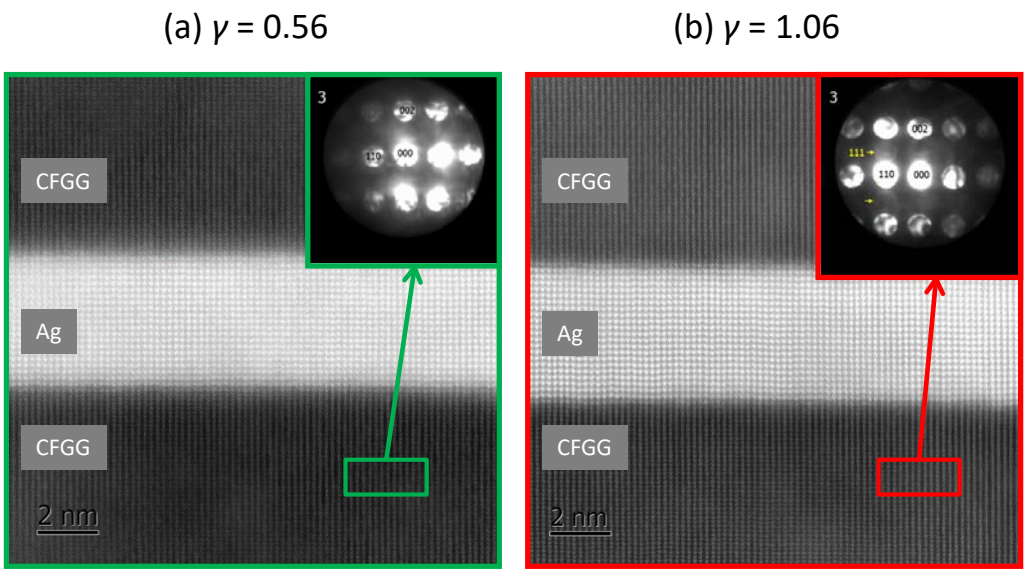


FIG. 4. HAADF-STEM lattice images of series-B GMR layer structures with (a) Ge-stoichiometric $Co_2Fe_{1.03}Ga_{0.41}Ge_\gamma$ film with $\gamma$ = 0.56 and (b) Ge-rich $Co_2Fe_{1.03}Ga_{0.41}Ge_\gamma$ film with $\gamma$ = 1.06. Inset of each figure shows CBED patterns for lower CFGG electrodes.

We now describe the Ge-composition dependence of the MR ratio of series-A, -B, and -C CPP-GMR devices. Figure 5 shows (a) MR ratios at 290 K for series-A samples

without NiAl insertion and series-B and -C samples with NiAl insertion as a function of the Ge composition $\gamma$ and (b) the MR curve for the maximum MR ratio observed for a series-C sample with $\gamma$ = 1.10. Comparison of the MR ratios for the series-A samples with those for the series-B and -C samples shows that the MR ratios were higher for all Ge compositions ranging from 0.56 to 1.06 when ultrathin NiAl layers were inserted at both interfaces of the Ag spacer. This result is consistent with that of a previous study [11], and possible origin for the enhancement of MR ratio is improvement of interfacial spin-dependent scattering by thin NiAl insertion [11]. Most importantly, the MR ratios increased with increasing $\gamma$ from 0.24 to 1.10 and reached a maximum value of 87.9% at Ge-rich composition $\gamma$ = 1.10. They then decreased rapidly to 35.3% with a further increase in $\gamma$ to 1.48. Typical MR curves with various Ge compositions are shown in Supplementary Data (see Fig. S4). The sharp-peaked structure in Fig. 5(a) contrasts with those obtained for MTJs having electrodes of $Co_2MnSi$ [26–28], $Co_2MnGe$ [27], or $Co_2(Mn,Fe)Si$ [29], in which the MR ratios were enhanced for a relatively wide range of Mn-rich compositions.

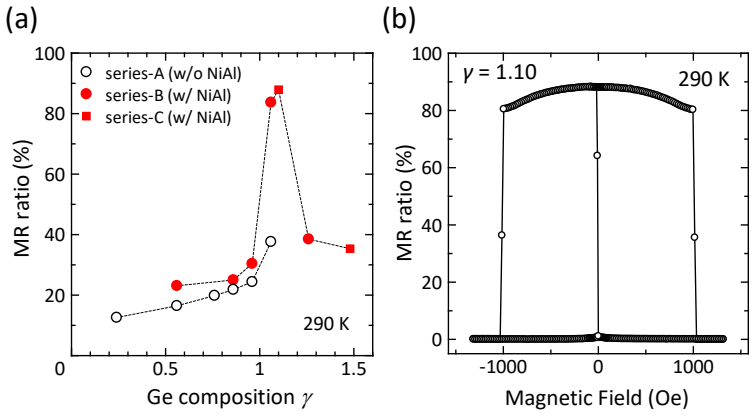


FIG. 5. (a) Ge-composition dependence of MR ratio for CFGG-based GMR devices. (b) MR curve with MR ratio of 87.9% at 290 K.

### D. Discussion

Now we will discuss the origin of the $\gamma$-dependence of the MR ratios in comparison with the theoretical spin polarization. As shown in Fig. 1(a), both $P_{\mathrm{th}}(spd)$ and $P_{\mathrm{th}}(sp)$ took the maximum at $\gamma = 0.56$. According to the Valet-Fert model [56], the MR ratio dominantly depends on either $[P_{\mathrm{th}}(spd)]^2$ or $[P_{\mathrm{th}}(sp)]^2$. Taking into consideration that $P_{\mathrm{th}}(spd)$ crosses zero at $0.24 < \gamma < 0.56$ and at $0.56 < \gamma < 0.96$, $[P_{\mathrm{th}}(spd)]^2$ decreases from 0.085 at $\gamma = 0.24$ to zero and then increases to the maximum value of 0.63 at $\gamma = 0.56$. As $\gamma$ further increases from 0.56 to 1.54, $[P_{\mathrm{th}}(spd)]^2$ decreases from 0.63 to zero and increases again to 0.20 at $\gamma = 1.54$. However, such a complicated $\gamma$ dependence of the MR ratios was not observed in Fig. 5(a), indicating that the MR ratio does not depend on $[P_{\mathrm{th}}(spd)]^2$. On the contrary, the $\gamma$ dependence of $[P_{\mathrm{th}}(sp)]^2$ can qualitatively explain the $\gamma$ dependence of the MR ratios, because it shows a single-peaked structure. This is reasonable because the electrical conduction in the GMR devices is mainly due to itinerant *s*- and *p*-like electrons, and the contribution from localized *d*-like electrons is negligible. The peaked structure seen in Fig. 5(a) is ascribed to that the formation of both $\mathrm{Co_{Fe}}$ and $\mathrm{Fe_{Co}}$ antisites is suppressed at

$\gamma \approx 1.1$.

However, the Ge composition that shows the maximum $P_{th}(sp)$ differs from the one that shows the maximum MR ratio. The value of $P_{th}(sp)$ is highest for the stoichiometric composition ($\gamma = 0.56$), whereas the MR ratio is highest near $\gamma = 1.1$. One possible reason for this difference is the $\gamma$-dependent degree of disorder, that is, as shown in Fig. 4, the CFGG film with $\gamma = 0.56$ was B2-ordered, and the one with $\gamma = 1.06$ was $L2_1$-orderd. On the other hand, the SSFU model assumes the thermodynamically stable atomic arrangement. This means that a complete $L2_1$-ordered structure is assumed for the stoichiometric composition of CFGG (The SSFU composition for $\gamma = 0.56$ is $[Co_2][Fe][Ga_{0.410}Ge_{0.560}Fe_{0.03}]$). In order to discuss the influence of $\gamma$-dependent degree of disorder on the MR ratio, we calculated $P_{th}(sp)$ for the SSFU composition with B2-type disorder, in which the atomic arrangement for the Fe site and (Ga,Ge) site is randomized (for detail, see §8 in Supplementary Data). Figure 6 shows $\gamma$ dependence of $P_{th}(sp)$ for the original SSFU model and that for the SSFU with B2-type disorder. When the B2-type disorder is introduced, the spin polarization decreases, especially at stoichiometric composition. However, the value of $P_{th}(sp)$ for the B2-type disorder at $\gamma = 0.56$ and that for the original SSFU model at $\gamma = 0.96$ are almost the same. Thus, the $\gamma$-dependent degree of disorder alone cannot explain the fact that the maximum MR ratio was obtained at Ge-rich composition.

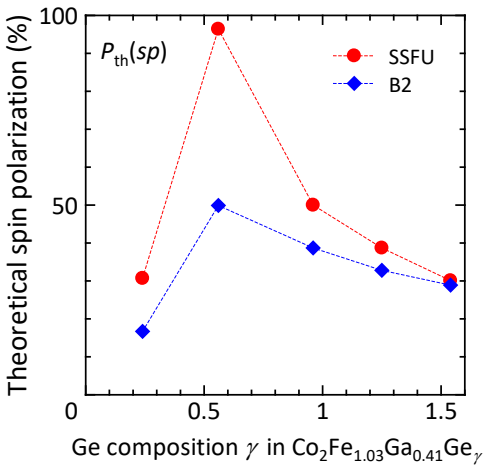


FIG. 6. Comparison of $\gamma$ dependence of $P_{th}(sp)$ for the original SSFU model and that for the SSFU with B2-type disorder.

Another possible reason is the reduction in the Ge composition of the CFGG electrodes in the CPP-GMR stacks due to diffusion of the Ge atoms during thermal annealing. In order to confirm this, we investigated depth profiles of Co, Fe, Ga, Ge, and Ag for a series-B GMR device with $\gamma$ = 1.06 observed through the energy dispersive x-ray spectroscopy (EDS) (see Fig. S6 in Supplementary Data). The film compositions of upper and lower CFGG, estimated from the EDS, were $Co_2Fe_1Ga_{0.25}Ge_{0.74}$ and $Co_2Fe_1Ga_{0.21}Ge_{0.64}$, respectively, whose Ga and Ge compositions are lower than those obtained from ICP analysis ($Co_2Fe_{1.03}Ga_{0.46}Ge_{1.06}$). Moreover, Ge concentration was slightly reduced at lower CFGG/NiAl/Ag interface. These results support the above Ge diffusion scenario.

## IV. CONCLUSION

We investigated the effect of off-stoichiometry on the half-metallic character of CFGG by using the Ge-composition dependence of $\mu_s$ and the MR ratio of CFGG-based CPP-GMR devices together with first-principles calculations. Theoretical calculations showed that spin polarization was the highest at stoichiometric composition $\gamma$ = 0.56 and that it

decreased in the off-stoichiometric compositions mainly due to the formation of $Co_{Fe}$ or $Fe_{Co}$ antisites, both of which destroy the half-metallic gap.

A maximum MR ratio of 87.9% at 290 K was obtained for a Ge-rich CFGG-based CPP-GMR device with $\gamma$ = 1.10, indicating that controlling the Ge-rich composition of CFGG is effective for suppressing harmful $Co_{Fe}$ and $Fe_{Co}$ antisites in CFGG-based CPP-GMR devices. This result is highly promising for applications to magnetic-field sensor with high sensitivity and low device resistance. The discrepancy between the Ge composition at which the highest theoretical spin polarization was obtained and that at which the highest MR ratio was obtained is due to the improved atomic arrangements in a Ge-rich CFGG film and a reduction of effective Ge composition by Ge diffusion in the GMR stacks.

**Acknowledgments**

The authors thank the late Prof. Masafumi Yamamoto for his fruitful discussions on the structural, magnetic, and electronic properties of Co-based Heusler alloys. This work was supported in part by the Japan Society for the Promotion of Science (KAKENHI: Grants 20H02174 and 20H02598) and the Center for Spintronics Research Network. H.S. thanks financial support from the Murata Science Foundation.

## References


[1] Takagishi M, Yamada K, Iwasaki H, Fuke H N, Hashimoto S 2010 *IEEE Trans. Magn.* **46** 2086

[2] Furubayashi T, Kodama K, Sukegawa H, Takahashi Y K, Inomata K and Hono K 2008 *Appl. Phys. Lett.* **93** 122507

[3] Furubayashi T, Kodama K, Nakatani T M, Sukegawa H, Takahashi Y K, Inomata K and Hono K 2010 *J. Appl. Phys.* **107** 113917

[4] Sakuraba Y, Izumi K, Iwase T, Bosu S, Saito K, Takanashi K, Miura Y, Futatsukawa K, Abe K and M. Shirai 2010 *Phys. Rev. B* **82**, 094444

[5] Hase N, Nakatani T M, Kasai S, Takahashi Y K and Hono K 2011 *J. Appl. Phys.* **109** 07E112

[6] Goripati H S, Hayashi M, Furubayashi T, Taniguchi T, Sukegawa H, Takahashi Y K and Hono K 2011 *J. Appl. Phys.* **110** 123914

[7] Sakuraba Y, Izumi K, Bosu S, Saito K and Takanashi K 2011 *J. Phys. D: Appl. Phys.* **44** 064009

[8]Sakuraba Y, Ueda M, Miura Y, Sato K, Bosu S, Saito K, Shirai M, Konno T J and Takanashi K 2012 *Appl. Phys. Lett.* **101** 252408

[9] Narisawa H, Kubota T and Takanashi K 2015 *Appl. Phys. Express* **8** 063008

[10] Du Y, Furubayashi T, Sasaki T T, Sakuraba Y, Takahashi Y K and Hono K 2015 *Appl. Phys. Lett.* **107** 112405

[11] Jung J W, Sakuraba Y, Sasaki T T, Miura Y and Hono K 2016 *Appl. Phys. Lett.* **108**, 102408

[12] Li S, Takahashi Y K, Sakuraba Y, Tsuji N, Tajiri H, Miura Y, Chen J, Furubayashi T and Hono K 2016 *Appl. Phys. Lett.* **108**, 122404

[13] Inoue M, Hu B, Moges K, Inubushi K, Nakada K, Yamamoto M and Uemura T 2017 *Appl. Phys. Lett.* **111** 082403

[14] Inoue M, Inubushi K, Mouri D, Tanimoto T, Nakada K, Kondo K, Yamamoto M and Uemura T 2019 *Appl. Phys. Lett.* **114** 062401

[15] Saenphum N, Chureemart J, Evans R F L, Chantrell R W, and Chureemart P 2021 *J. Phys. D: Appl. Phys.* **54** 395004

[16] Zhang L, Zhang B Y, Jiang L W, and Zheng Y S 2022 *J. Phys. Condens. Matter.* **34** 204003

[17] Fathoni K B, Sakuraba Y, Miura Y, Sasaki T, Nakatani T, and Hono K 2022 *J. Phys. D: Appl. Phys.* **55** 125001

[18] Kübler J, Williams A R and Sommers C B 1983 *Phys. Rev. B* **28** 1745

[19] Ishida S, Fujii S, Kashiwagi S and Asano S 1995 *J. Phys. Soc. Jpn.* **64** 2152

[20] Picozzi S, Continenza A and Freeman A J 2002 *Phys. Rev. B* **66** 094421

[21] Galanakis I, Dederichs P H and Papanikolaou N 2002 *Phys. Rev. B* **66** 174429

[22] Shakil M, Sadia H, Khan M I, Gillani S S A, Gadhi M A, and Boukhris I 2022 *Physica B: Condens. Matter*. **625** 413524

[23] Webster P J 1971 *J. Phys. Chem. Solids* **32** 1221

[24] Picozzi S, Continenza A and Freemanet A J 2004 *Phys. Rev. B* **69** 094423

[25] Miura Y, Nagano K and Shirai 2004 *Phys. Rev. B* **69** 144413

[26] Ishikawa T. Liu H-x, Taira T, Matsuda K-i, Uemura T and Yamamoto M, *Appl. Phys. Lett.* **95** 232512

[27] Yamamoto M, Ishikawa T, Taira T, Li G-f, Matsuda K-i and Uemura T 2010 *J. Phys.: Condens. Matter.* **22** 164212

[28] Liu H-x, Honda Y, Taira T, Matsuda K-i, Arita M, Uemura T and Yamamoto M 2012

*Appl. Phys. Lett.* **101** 132418

[29] Liu H-x, Kawami T, Moges K, Uemura T, Yamamoto M, Shi F and Voyles P M 2015 *J. Phys. D: Appl. Phys.* **48** 164001

[30] Li G-f, Honda Y, Liu H-x, Matsuda K-i, Arita M, Uemura T, Yamamoto M, Miura Y, Shirai M, Saito T, Shi F and Voyles P M 2014 *Phys. Rev. B* **89** 014428

[31] Moges K, Honda Y, Liu H-x, Uemura T, Yamamoto M, Miura Y and Shirai M 2016 *Phys. Rev. B* **93** 134403

[32] Wüstenberg J-P, Fetzer R, Aeschlimann M, Cinchetti M, Minár J, Braun J, Ebert H, Ishikawa T, Uemura T and Yamamoto M 2012 *Phys. Rev. B* **85** 064407

[33] Asakura D, Koide T, Yamamoto S, Tsuchiya K, Shioya T, Amemiya K, Singh V R, Kataoka T, Yamazaki Y, Sakamoto Y, Fujimori A, Taira T and Yamamoto M 2010 *Phys. Rev. B* **82** 184419

[34] Singh V R, Verma V K, Ishigami K, Shibata G, Kadono T, Fujimori A, Asakura D, Koide T, Miura Y, Shirai M, Li G-f, Taira T and Yamamoto M 2012 *Phys. Rev. B* **86** 144412

[35] Singh V R, Verma V K, Ishigami K, Shibata G, Fujimori A, Koide T, Miura Y, Shirai M, Ishikawa T, Li G-f and Yamamoto M 2015 *J. Appl. Phys.* **117** 203901

[36] Ouardi S, Fecher G H, Chadov S, Balke B, Kozina X, Felser C, Taira T and Yamamoto M 2013 *Appl. Phys. A: Mater. Sci. Process.* **111** 395

[37] Kozina X, Karel J, Ouardi S, Chadov S, Fecher G H, Felser C, Stryganyuk G, Balke B, Ishikawa T, Uemura T, Yamamoto M, Ikenaga E, Ueda S and Kobayashi K 2014 *Phys. Rev. B* **89** 125116

[38] Fetzer R, Ouardi S, Honda Y, Liu H-x, Chadov S, Balke B, Ueda S, Suzuki M, Uemura T, Yamamoto M, Aeschlimann M, Cinchetti M, Fecher G H and Felser C

2015 *J. Phys. D: Appl. Phys.* **48** 164002

[39] Li T, Yan W, Zhang X, Hu B, Moges K, Uemura T, Yamamoto M, Tsujikawa M, Shirai M and Miura Y 2020 *Phys. Rev. B* **101** 174410

[40] Hohenberg P and Kohn W 1964 *Phys. Rev.* **136** B864

[41] Kohn W and Sham L J 1965 *Phys. Rev.* **140** A1133

[42] Kresse G and Hafner J 1963 *Phys. Rev. B* **47** 558(R)

[43] Kresse G and Furthmüller J 1996 *Phys. Rev. B* **54**, 11169

[44] Kresse G and Furthmüller J 1996 *Comput. Mater. Sci.* **6**, 15

[45] Blöchl P E 1994 *Phys. Rev. B* **50**, 17953

[46] Monkhorst H J and Pack J D 1976 *Phys. Rev. B* **13** 5188

[47] Perdew J P, Burke K and Ernzerhof M 1996 *Phys. Rev. Lett.* **77** 3865

[48] Korringa J 1947 *Physica* **13** 392

[49] Kohn W and Rostoker N 1954 *Phys. Rev.* **94** 1111

[50] Shiba H 1971 *Prog. Theor. Phys.* **46** 77

[51] Soven P 1970 *Phys. Rev. B* **2** 4715

[52] Akai H 1989 *J. Phys.: Condens. Matter* **1** 8045

[53] Filippetti A, Pemmaraju C D, Sanvito S, Delugas P, Puggioni D and Fiorentini V 2011 *Phys. Rev. B* **84** 195127

[54] Koelling D D and Harmon B N 1977 *J. Phys. C: Solid State Phys.* **10** 3107

[55] Hülsen B, Scheffler M and Kratzer P 2009 *Phys. Rev. B* **79** 094407

[56] Valet T and Fert A 1993 *Phys. Rev. B* **48** 7099